7 May 2026

DFT-based grand canonical study of the stability of crystalline battery materials under operating conditions

Johannes Döhn, Axel Groß

Abstract

High-throughput computational studies can significantly aid in the identification of crystalline battery materials with improved properties. Here we present a density functional theory-based numerical study addressing the stability of crystalline materials for chloride ion batteries under operating conditions using a grand canonical approach. Cl ion batteries have emerged at the science stage as a potential energy storage technology promising enhanced energy density based on safe and environmentally benign chemistries. Although significant progress has been achieved in this field recently, the discovery of potential materials is only in its infancy. In the present work, we computationally address the materials class of chloride perovskites for the development of new chloride ion battery materials. 18782 intercalation configurations for each of a total of 205 different compounds are evaluated employing a state-of-the-art machine learning interatomic potential and periodic density functional theory calculations. For the analysis, a particular focus is put on the comprehensive investigation with grand canonical diagrams. As this method inclusively covers the thermodynamic relations between the pristine compounds, its intercalation configurations, and potential conversion products under varying electrochemical conditions, we believe this approach is of great aid in the theoretical description and identification of potential materials. Our investigation resulted in the proposal of 23 solid electrolyte materials for further investigation. Six compounds exhibit reversible Cl intercalation/deintercalation, i.e. they are in principle suitable as cathode materials, however, the reversible cycling should only be possible in a rather narrow potential window.

DFT-based grand canonical study of the stability of crystalline battery materials under operating conditions

Johannes Döhn[†] and Axel Groß[*,†,‡]

[†]*Institute of Theoretical Chemistry, Ulm University, Oberberghof 7, 89081 Ulm, Germany*

[‡]*Helmholtz Institute Ulm (HIU) for Electrochemical Energy Storage, Helmholtzstraße 11, 89081 Ulm, Germany*

E-mail: axel.gross@uni-ulm.de

Abstract

High-throughput computational studies can significantly aid in the identification of crystalline battery materials with improved properties. Here we present a density functional theory-based numerical study addressing the stability of crystalline materials for chloride ion batteries under operating conditions using a grand canonical approach. Cl ion batteries have emerged at the science stage as a potential energy storage technology promising enhanced energy density based on safe and environmentally benign chemistries. Although significant progress has been achieved in this field recently, the discovery of potential materials is only in its infancy. In the present work, we computationally address the materials class of chloride perovskites for the development of new chloride ion battery materials. 18782 intercalation configurations for each of a total of 205 different compounds are evaluated employing a state-of-the-art machine learning interatomic potential and periodic density functional theory calculations. For the analysis, a particular focus is put on the comprehensive investigation with grand canonical diagrams. As this method inclusively covers the thermodynamic relations between the pristine compounds, its intercalation configurations, and potential conversion products under varying electrochemical conditions, we believe this approach is of great aid in the theoretical description and identification of potential materials. Our investigation resulted in the proposal of 23 solid electrolyte materials for further investigation. Six compounds exhibit reversible Cl intercalation/deintercalation, i.e. they are in principle suitable as cathode materials, however, the reversible cycling should only be possible in a rather narrow potential window.

Introduction

Current state-of-the-art battery technology based on the shuttle of Li-ions has taken a long route towards the present large scale production and application.[1–4] Although Li being the lightest and most electropositive metal and, thereby, the natural candidate for electrochemical energy storage, its high reactivity within air or aqueous environments renders its application rather difficult. It took one and a half decades of intense research from the first successfully demonstrated battery prototype based on the Li/TiS_2 cell in 1976[5] over the introduction of $LiCoO_2$ at the cathode[6] and certain carbonaceous structures at the anode side until the reactive Li was completely tamed and the first commercially suitable prototype of a Li-ion cell was released by Sony in 1991.[7,8] And yet, another 20 years and the introduction of improved cathode materials, namely NMC and NCA,[9–11] had to go by until cell manufacturing and handling had reached a stage which enables batteries to be produced sufficiently cheap and efficient to make them available in quantities and at prices that allow large scale applications as in electric vehicles or stationary storage systems.[12,13] That being said, recent growing sensitivity for sustainability in combination with ramped up cell production and the ever growing need for energy storage has impacted the research focus. And again, another material, namely $LiFePO_4$ entered the realm of commercial Li-ion cell production, as it relies on abundant precursors only.[14–16]

The just described evolution of Li-ion technology, although only mentioning the major milestones, clearly emphasizes that the introduction of new materials levered its performance to a level which is nowadays considered standard, opening up all possibilities of present technology. Similar examples can be found across the entire realm of science and technology, rendering material development the ultimate core of technological innovation.[17–22] Given the utmost importance of energy storage for worldwide energy transition and the saturation in the progress of Li-ion batteries, such innovation is clearly needed in the development and advancement of novel storage technologies. The Cl ion battery (CIB) is such a novel approach that belongs to the class of so-called post or beyond-lithium battery systems.[23,24]

Being among the most electronegative elements, Cl exhibits high affinity towards chemical reaction with almost any other element of the periodic table forming a multitude of diverse compounds. Smart choice of battery materials, thus, promises enhanced energy density based on safe and environmentally benign chemistries.[25,26] As the proof of concept for a CIB has been delivered only in 2014,[27] one could argue that the research for CIBs is at the stage where it was in the 1980s for Li-ion batteries. Clearly, the discovery of potential materials is only in its infancy and the entire chemical space is still open for exploration.

Nonetheless, the development of novel materials is not a straight forward task, as the described evolution towards the modern Li-ion battery proves. Experimental trial and error procedures, although being conducted by excellent scientists, are tedious and time consuming rendering the space of potential candidate materials by far too large for any systematic exploration. Fortunately, this route can potentially be cut short by modern computational investigations. The in-silico determination of intrinsic materials properties oftentimes being supplemented by the utilization of large data repositories allows the suggestion of potentially feasible materials within a time frame several orders of magnitude shorter than within the experimental approach.[28,29] Such studies are typically based on density functional theory calculations (DFT) and have recently been more and more complemented and accelerated by machine learned interatomic potential (MLIP) calculations. In fact, recent breakthroughs in the creation of universal potentials have made it possible to assess ground state energies at almost DFT-accuracy but with gigantic savings in computational effort, elevating the possibilities of theoretical materials exploration to a new stage.[30]

For the present study we employed a grand canonical approach[31–34] using a combination of DFT and MLIP calculations in order to explore the chemical space of chloride perovskites —i.e., $ABCl_3$ with A and B being potentially any element of the periodic table —for its potential suitability in CIBs. Chloride perovskites (as well as its bromide and iodide equivalents) have been the booming materials for photovoltaic applications for over a decade.[35] A great deal of their success is ascribed to their high flexibility and tolerance towards lat-

tice defects or imperfections including the facile diffusion of ionic species[36,37] —properties that are of utmost importance in batteries, too. In batteries the defects of halide ions correspond to certain intercalation configurations, i.e., Cl vacancies or interstitials. Thus, in this work we discuss how such Cl intercalation configurations determine properties that are relevant for electrode or solid electrolyte materials which could potentially be used in CIBs. In this regard, as electrodes are the active materials of the battery, they require the existence of stabilized Cl loadings at varying concentration to establish the capacity of the system. The theoretical open-circuit voltage of the battery is in this terminology determined by the chemical potential for chlorination/dechlorination of its electrodes.[38,39] Opposed to that, solid electrolyte materials are non-active, i.e., they do not take part in the electrochemical battery reactions, which precludes the presence of such stable intercalation configurations. In this case, the theoretical stability window is limited by the spread of the chlorination/dechlorination chemical potential. In this study, the investigation of such chlorinated/dechlorinated perovskite materials $ABCl_{3\pm x}$ was approached by the evaluation of roughly 4 million atomic configurations of over 200 different cation combinations A and B by DFT and MLIP calculations.

Furthermore, electrode and solid electrolyte materials must be stable with respect to potential decomposition under operating conditions. In a grand canonical approach, these operating conditions enter via the chemical potentials of the involved species which are a function of, among others, the applied potential and the concentration of the involved species.[40–42] Thus, we elucidate how materials databases can be used to obtain meaningful insights on the stability at varying Cl loadings and electrochemical conditions. A particular focus is put on the analysis with grand canonical diagrams, frequently applied using the concepts of ab initio thermodynamics or the computational hydrogen electrode.[31,32,34,43] In the battery community, this approach has typically been used for stability investigations of Li-ion solid electrolyte materials,[44–46] but was recently applied to successfully explain the degradation behavior of a CIB electrode material, too.[47] Grand canonical diagrams contain in a com-

pact form information on the relative stability of the pristine and chlorinated/dechlorinated materials as well as potential decomposition products at varying potentials and Cl loadings. They can therefore help to predict if chlorination/dechlorination takes place and whether topotactic or conversion reactions are to be expected. Furthermore, relevant properties as the open circuit voltage or the electrochemical stability window can be read off directly from the diagrams. A quick glimpse on such a diagram therefore reveals a materials' potential as electrode or solid electrolyte in a CIB. Here, we create the grand canonical diagrams of all 205 investigated perovskites and discuss the most promising materials in greater detail, eventually providing suggestions of candidate materials for CIBs but also offering a blueprint for similar studies on other interesting materials classes.

Theoretical and Methodological Considerations

From a solid state chemistry perspective the working principle of CIBs is rather simple, although one has to get used to the reversed logic related to the anionic nature of Cl^- compared to the ultimate reference Li^+ as for instance described by Euchner and Groß.[38] In principle, regarding the electrode materials independently, the Cl atom is more strongly bound in the anode than in the cathode —quite opposite to the Li-ion case. In terms of thermodynamic quantities this is expressed by the fact that $\mu_{Cl}^{A} < \mu_{Cl}^{C}$, where $\mu_{Cl}^{A,C}$ is the chemical potential of Cl in the anode and the cathode, respectively (cf. Fig. 1). In a battery setup though, the anode and the cathode are not independent objects but are connected by the electrolyte that needs to be Cl^- conducting and electronically insulating. Hence, on statistical average the Cl ions will travel towards the electrode with the stronger bond and, thereby, separate charges between the electrodes. Under open circuit conditions the charge separation will compromise the initial driving force for the diffusion until some equilibrium in the Cl^- distribution across the cell is established, and in particular $\tilde{\mu}_{Cl^-}^{A} = \tilde{\mu}_{Cl^-}^{C}$. In this expression the electrochemical potential of Cl^- can be expressed as the sum of the

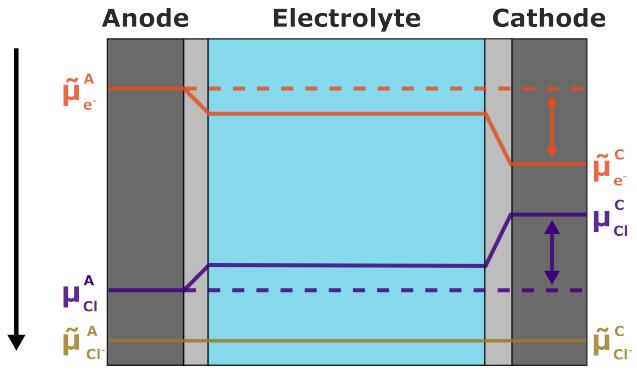

Fig. 1: Potential curves between the anode and cathode within a CIB at open circuit conditions. The potential changes within the electric double layer are schematically indicated by linear slopes which do not represent any physical foundation. The figure is based on earlier work by Euchner and Groß.[38,39]

chemical potential of Cl and the electrochemical potential of the corresponding electron, i.e., $\tilde{\mu}_{Cl^-} = \mu_{Cl} + \tilde{\mu}_{e^-}$. Thus, the open circuit voltage φ_{OCV}, i.e. the driving force for the flow of electrons in the external circuit,[48] can be traced back to the difference in the chemical potential of Cl in the corresponding electrodes

$$\varphi_{OCV} = \frac{\tilde{\mu}^A_{e^-} - \tilde{\mu}^C_{e^-}}{e} = \frac{\mu^C_{Cl} - \mu^A_{Cl}}{e}, \tag{1}$$

where e denotes the elemental charge and $\mu^{A,C}_{Cl}$ are the Cl chemical potentials associated with the insertion/deinsertion of Cl into/from the electrodes. Furthermore, note that under equilibrium conditions the electric double layers are overall charge neutral so that there are no macroscopic electric fields in the bulk electrodes and the bulk electrolyte. This also means that the electrochemical potentials have to be constant in each material so that they can be used to characterize the state of these materials, which is of great importance for the sake of modeling. The electric fields and the corresponding variations in the chemical potential of the electrons across the cell must be solely attributed to the formation of the electric double layer at the electrode-electrolyte interfaces —the corresponding potential drop being schematically indicated by the slopes in Fig. 1.[38,39]

Fig. 1 in conjunction with equation 1 implies that the boundaries for the chemical potential throughout the entire system are given by the electrochemically active species, i.e. μ_{Cl}^{A} and μ_{Cl}^{C}, which means that the chemical potential associated with the oxidation and reduction of the electrolyte needs to fulfill

$$\mu_{Cl}^{SE,red} < \mu_{Cl}^{A} \text{ and } \mu_{Cl}^{C} < \mu_{Cl}^{SE,ox}, \tag{2}$$

where $\mu_{Cl}^{SE,red}$ and $\mu_{Cl}^{SE,ox}$ are associated with the unwanted Cl intercalation/deintercalation into/from the solid electrolyte. If this was not the case, the electrolyte would represent a Cl source that is reduced by the anode or a Cl sink that is oxidized by the cathode, instead of only transferring the ions.[49] The spread of $\mu_{Cl}^{SE,ox}$ and $\mu_{Cl}^{SE,red}$ is typically called stability window. Eventually, equations 1 and 2 fully determine the intercalation thermodynamics of battery materials and they can be used to classify potential battery materials accordingly.

It is obvious that the chlorination/dechlorination chemical potential is of outstanding importance for the electrochemical description of CIB materials. In this study we investigate chloride perovskites with the general formula $ABCl_3$. In terms of atomistic calculations the chemical potential $\mu_{Cl}^{vac/int}$ associated with chlorination/dechlorination of such a compound is derived by the energy gain/loss concomitant to the addition/removal of a Cl atom

$$\mu_{Cl}^{vac/int} = \pm\frac{1}{x}\left\{E^{ABCl_{3\pm x}} - E^{ABCl_3}\right\}, \tag{3}$$

where E can for instance be obtained from DFT or MLIP calculations. Equation 3 reflects that within the atomistic picture the oxidation and reduction of anode, cathode and solid electrolyte materials during battery operation corresponds to nothing else but the creation and annihilation of Cl vacancies and Cl interstitials, i.e., the intercalation and deintercalation of Cl. Thus, regardless of whether such a change in Cl loading is wanted as in the case of the electrodes or unwanted as in the case of solid electrolytes, the thermodynamic transition level given by equation 3 eventually determines the suitability of potential CIB

materials. Additionally, vacancies and interstitials are the potentially mobile species in any of the discussed battery components, so their density is strongly connected to the mobility of the ionic species.[50] Conclusively, the relevance of intercalation configurations $ABCl_{3\pm x}$ in equation 3 for the understanding of battery materials within the atomistic picture can hardly be overemphasized and it can be seen as one of the main goals of atomistic high throughput calculations to classify materials accordingly.[51–53]

Generally, the perovskite geometry is characterized by corner-sharing Cl octahedra around the central B-site cation with the A-site cations filling the voids within this scaffold (Fig. 2 a). The ideal cubic perovskite structure is highly symmetric, but many real compounds are subject to distortions of this highly symmetric phase, most famously recognized being the octahedral tilting described by A. M. Glazer.[54–56] DFT investigations revealed that such distortions may lower the energy by several 100 meV/atom obliging their consideration.[57,58] This aspect is of even greater importance when vacancies/interstitials are considered as their introduction may break the symmetry of the cell and lead to unreliable chlorination/dechlorination energies when compared to wrong base geometries.[59] Hence, in the present study we considered the cubic phase ($Pm\bar{3}m$), the most common tilting configurations with symmetries I4/mcm, P4/mbm, Imma, $R\bar{3}c$, Pnma and $Im\bar{3}$, and the shift of the A or the B-site cation corresponding to the symmetry P4mm.[58,60,61] To model $ABCl_3$ we used supercells of 40 atoms as depicted in Fig. 2 b) and corresponding to eight formula units. The computational structures were generated using the code provided by Xie and coworkers.[57]

The modeling of vacancies/interstitials is generally a quite expensive task. As it is by no means a priori clear which exact intercalation configuration determines the property of interest,[62] in principle every possible configuration has to be considered, blowing up the number of necessary calculations tremendously. This is even more far-reaching in the case of anionic species, as Cl^- with formal oxidation state -1 typically outnumbers the cationic species, giving rise to an even larger number of potential combinations. For the present study

we considered single/double vacancies and single/double interstitials in the above described supercells as well as any combination thereof leading to eight different types of Cl loadings (Fig. 2 a). Vacancies were modeled by simply removing a Cl atom and interstitials were modeled by considering two Cl atoms close to an originally singly occupied Cl-site (Fig. 2 c). Note that although the Cl ion is the chemically relevant species, the supercells have to be kept charge neutral and the electronic distribution is given as a result of the self-consistent electronic structure calculations. The atomic simulation environment (ASE) was employed to generate the input structures.[63] For the cubic perovskite, the total number of unique configurations which can be generated in the described way for each type of defect is shown in the table in Fig. 2 a). For the other structural types only the total number is indicated in brackets in Fig. 2 b), the number being higher for the less symmetric geometries. Note that this approach includes single and double Frenkel defects but also Cl loadings that slightly change the stiochiometry of the compound. Cationic defects were not considered. Eventually, in the described way, in total 18782 configurations with stiochiometries $ABCl_{3\pm x}$ with $x \in \left\{0, \frac{1}{24}, \frac{1}{12}\right\}$ are investigated for each given combination of cations A and B.

Such a number of input geometries is clearly too large for a DFT-only approach. Remedy is found in MLIPs, so far the perhaps most influential contribution of artificial intelligence to computational materials science.[30,64] Initially being successfully developed for specific materials or chemistries only, the trend has most lately shifted towards the creation of universal models with the capability to describe materials in a multitude of structures throughout the entire periodic table and with respect to various properties.[65] In particular, a very recent benchmark study has demonstrated that such potentials are able to describe defective materials at reasonable accuracy but orders of magnitude faster than DFT[66] —a finding for which we provide further supporting evidence in the present study. Here, we employed the universal model MACE-MPA-0, which is trained on the MPtr-dataset[67] and the Alexandria database.[68] The model shows reasonable accuracy for structure predictions (E_{MAE} = 28 meV) compared to DFT as benchmarked by the Matbench Discovery project.[69] For each

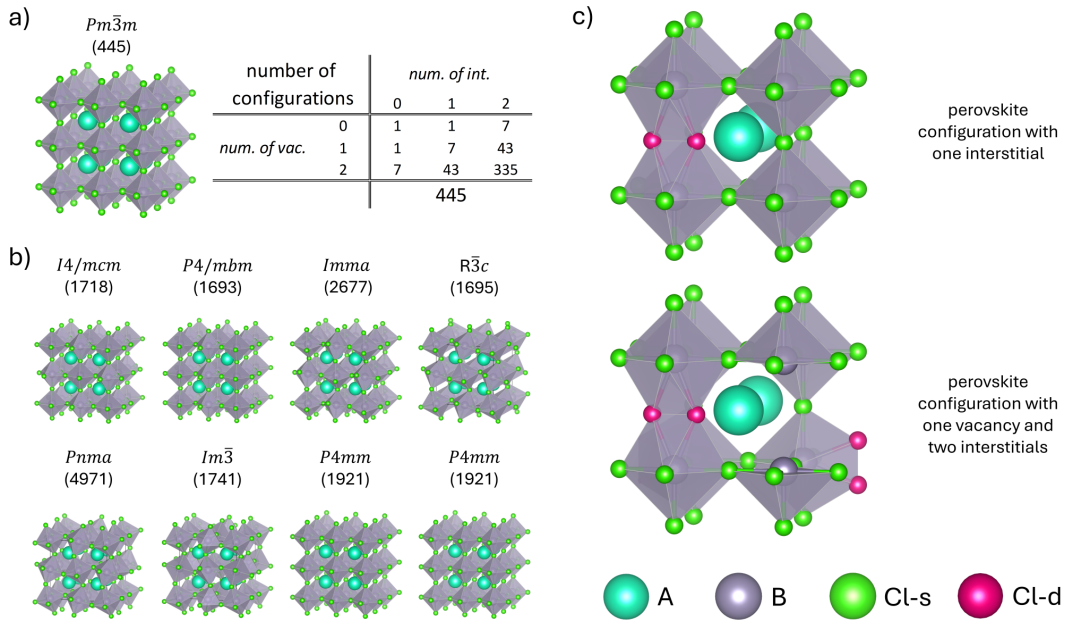

Fig. 2: a) Visualization of the ideal perovskite. The table contains the number of unique input configurations for each considered type of Cl loading; in total 445. b) Visualization of distorted perovskite symmetries. The number in the brackets gives the total number of unique input configurations. c) Exemplary visualization of two intercalation configurations belonging to two different types of Cl loading. One containing an interstitial Cl atom and the other containing two interstitials and one vacancy. The color distinguishes between the singly occupied Cl-s sites (green) and the doubly occupied Cl-d sites (rose).

cation combination A and B we used the MLIP to optimize the geometry of the described 18782 intercalation configurations until the forces and stresses were smaller than 0.05 eV/Å employing the FrechetCellFilter provided by ASE.[63]

In order to obtain accurate DFT energies, we evaluated the configuration with the lowest MLIP energy of each type of Cl loading employing the exchange-correlation functional suggested by Perdew, Burke, and Ernzerhof[70] (PBE) as implemented in the Vienna Ab Initio Simulation Package (VASP).[71–73] The ionic cores were treated with the Projector Augmented Wave method.[74] The energy cut-off (520 eV) and the number of k-points (mostly 3x3x3) were chosen such that the energies converged within a few meV/atom compared to more refined settings. The structures were reoptimized until the entries of the stress tensor and all forces were below 0.05 eV/Å without constraining any internal degree of freedom. All calculations were performed spin polarized with ferromagnetic initialization for d- and f-elements.

The obtained DFT energies can be used to assess the stability of the considered materials by employing the concept of the energy above hull E_{hull}, which describes the energetic difference of a certain atomic configuration (i.e., a material) to the energetically most favourable configuration with the same stoichiometry.[75] The calculational procedure has been described in greater detail in recent publications.[47,58] Note that in the present study a correction for the DFT predicted Cl_2-overbinding was applied.[76] Potential allotropes and decomposition products were taken from a database of roughly 115 000 compounds, which comprises the convex hull (i.e., all compounds with $E_{hull} = 0$ eV) of the entire chemical space.[77,78] As in the present study configurations with varying Cl content exposed to various electrochemical conditions have to be examined with respect to their stability, we screened the database accordingly.

The chlorinated/dechlorinated perovskite configurations are most illustratively related to each other and to potential allotropes or decomposition products with the help of the grand canonical approach.[34,40,41,43–47] Conceptually, it ascribes the stoichiometric difference of Cl atoms of the analyzed configurations to a Cl reservoir, i.e., one of the electrodes that takes up or releases Cl ions in the case of CIBs. A qualitative example is shown in Fig. 3. The fundamental entity of interest here is the formation energy

$$E_f \;=\; E - \sum_i \mu_i \; N_i, \tag{4}$$

where E is the ground state energy of the configuration of interest and μ_i and N_i are the chemical potential and the stoichiometric number of each elemental species, μ_i corresponding to the most stable form of the species. As visualized in Fig. 3 one can deduce statements on the relative stability at a given value of μ_{Cl} by comparing E_f of a set of configurations. The intersection of two lines (marked by a blue circle in Fig. 3) yields the thermodynamic transition level, i.e. the chemical potential μ_{Cl} at which the most stable configuration changes. Concerning battery materials, this is exactly the value which enters equations 1 and 2, where

it can be clearly distinguished whether topotactic intercalation or decomposing conversion reactions are to be expected at a certain transition point. Furthermore, by relating the transition point to a reference system, the difference that appears in equation 1 or the stability window given by equation 2 can be read off the graph directly. Li metal is often used as anode material in Cl-ion batteries which transforms to LiCl upon discharge, i.e., the Cl-ion battery is driven by the energy gain of LiCl formation. Hence, LiCl has been established as reference,[79] although the use of Sn and Ag are also frequently reported. In the present study we stick with LiCl as reference and identify the Cl-poor limit, i.e., the level at which the investigated perovskite is maximally reduced, with the Cl chemical potential associated with LiCl formation μ_{Cl}^{LiCl}. Numerically, the value of μ_{Cl}^{LiCl} is shifted by -4.27 eV compared to $\frac{1}{2}\mu_{Cl_2}^0$ (including the correction discussed above), where $\mu_{Cl_2}^0$ is the chemical potential associated with the gas phase at standard conditions. We also use gas phase Cl_2 for normalization according to $\Delta\mu_{Cl} = \mu_{Cl} - \frac{1}{2}\mu_{Cl_2}^0$. Please note that in a battery setup the Cl-rich limit does not necessarily correspond to $\Delta\mu_{Cl} = 0$ as the conditions may differ significantly from standard conditions. Furthermore, for better comparison to experimental results we relate μ_{Cl} to the experimentally accessible electrode potential φ vs. Li/Li^+ via

$$\mu_{Cl} = \mu_{Cl}^{LiCl} + e\ \varphi. \tag{5}$$

This also means that in line with equation 1 the open circuit potential φ_{OCV} vs. Li/Li^+ corresponding to a certain thermodynamic transition is directly accessible via the diagram. The same is true for the stability window in V vs. Li/Li^+. Please note that in the field of CIBs the expression Li/Li^+ refers to the formation of LiCl as to be distinguished from common terminology in discussions on Li-ion batteries where it refers to metallic Li.

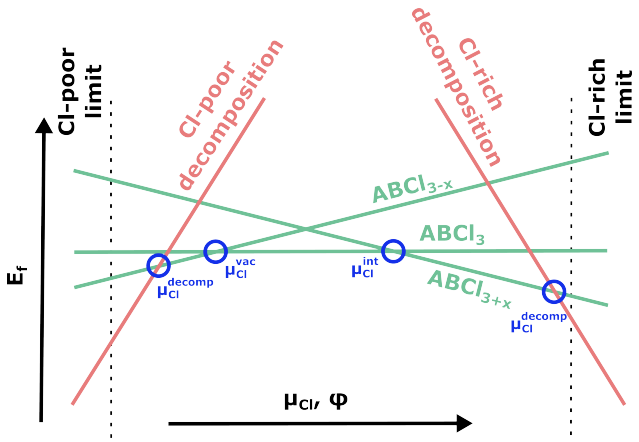

Fig. 3: Schematic representation of a grand canonical diagram for the system $ABCl_3$ connected to a Cl reservoir including the perovskite at varying Cl loading (green) and decomposition products (red). The blue circles indicate the transition points between two phases.

Eventually, a rather technical remark: As N_A and N_B are not varied in the presented approach, a more convenient expression can be derived for practical purposes. Relating E_f of the configuration of interest to the pristine perovskite, equation 4 becomes

$$E_f \; - \; E_f^{ABCl_3} \; = \; E \; - \; E^{ABCl_3} \; + \; \mu_{Cl} \; \Delta N_{Cl}, \tag{6}$$

where ΔN_{Cl} is the difference in the number of Cl atoms with respect to the pristine perovskite $ABCl_3$ which is supplied or taken up by the Cl reservoir. Equation 6 is technically quite appealing as the right side avoids any ambiguities with respect to formation energies and only requires direct DFT data as input.

Results

The present study is dedicated to finding chloride perovskites with suitable intercalation configurations, i.e., they suggest potential for battery materials, preferentially with improved properties. As input stiochiometries, 136 potentially stable perovskite-like compounds $ABCl_3$ were found in the Alexandria database.[77,78,80] This list comprises all compounds found by a prior comprehensive high-throughput study.[81] Additionally, we evaluated the recently sug-

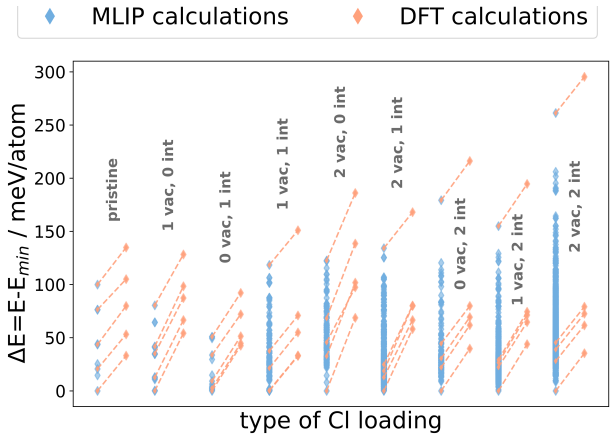

Fig. 4: MLIP energies of all 18782 evaluated configurations (blue) and DFT energies of 45 randomly chosen configurations (orange) normalized to the minimum energy for each type of Cl loading. Although the absolute values differ the energetic order does not change when moving from MLIP to DFT.

gested new tolerance factor,[82] a machine learned stability descriptor which was shown to predict stable chloride perovskites with 90% success, only requiring the ionic radii and oxidation states of the involved species as input.[83] Disregarding toxic and very rare elements[58] we ended up with 205 combinations A and B (Tab. S1) all of which were investigated as described above.

Fig. 4 depicts the results of the 18782 MLIP calculations of $NaMnCl_3$ as example compound. The pristine compound is predicted to be energetically most favourable in Pnma symmetry, the cubic configuration being less favourable by almost 100 meV/atom. For certain intercalation configurations the energetic spread ΔE, that is the energetic difference to the most favourable configuration, is considerably higher —at most up to 250 meV for the structures with two vacancies and two interstitials. We made similar observations throughout many of the investigated compounds. In certain cases, the spread is even as high as 1 eV/atom. This is quite significant. Consequently, the spread of ΔE among the various symmetries and intercalation configurations clearly emphasizes the necessity to investigate all possible configurations to obtain meaningful results on the equilibrium state. In other words: By random investigation of only a small set of the possible configurations one may incorporate errors as large as these values.

The MLIP results were reassessed by DFT geometry optimizations on 45 randomly chosen configurations as depicted in Fig. 4 as well. The data points of the MLIP and the DFT datasets which correspond to the same input configuration are connected by dashed lines. The analysis reveals that the absolute results of the MLIP and the DFT calculations may differ by up to 50 meV/atom in the case of $NaMnCl_3$. Nonetheless, the order of the input geometries with respect to ΔE is preserved when moving from MLIP to DFT indicating that the relative stability is well reproducible by the employed MLIP, even for chlorinated/dechlorinated configurations. Similar analyses were conducted on altogether 20 randomly chosen compounds, confirming the just presented results – the energetic order only changed in rougly 10 % of the investigated cases when moving from MLIP to DFT. After all, the discussed benchmark on the used MLIP justifies the approach taken here, i.e. screening all potential configurations with MLIP and only evaluating the most stable ones with DFT to obtain accurate ground state energies. This is a remarkable result: The used strategy allows to evaluate defects to an extend which would not be possible by the traditional DFT-only approach.

Carrying on, for each compound $ABCl_3$ and each type of Cl loading we evaluated the configuration with the lowest MLIP energy employing DFT, the corresponding results being discussed in the rest of the section. Note that the geometry optimization algorithms as implemented in ASE or VASP are designed to find the next local minimum of the potential energy surface, not to overcome energetic barriers. This means that if a given geometry collapses during relaxation, it was not in or close to a local minimum and is, therefore, very unlikely to represent a stable or even metastable material. Hence, it is most interesting whether the typical perovskite geometry, i.e., the scaffold of corner-sharing B-centered octahedra having A atoms in their voids, is preserved during geometry relaxation or not. Putting a hard criterion to answer this question, which could for instance be based on bond lengths and angles, is a highly difficult task, especially given the multitude of distinct compounds and the variety of investigated defects. To circumvent related issues, we inspected

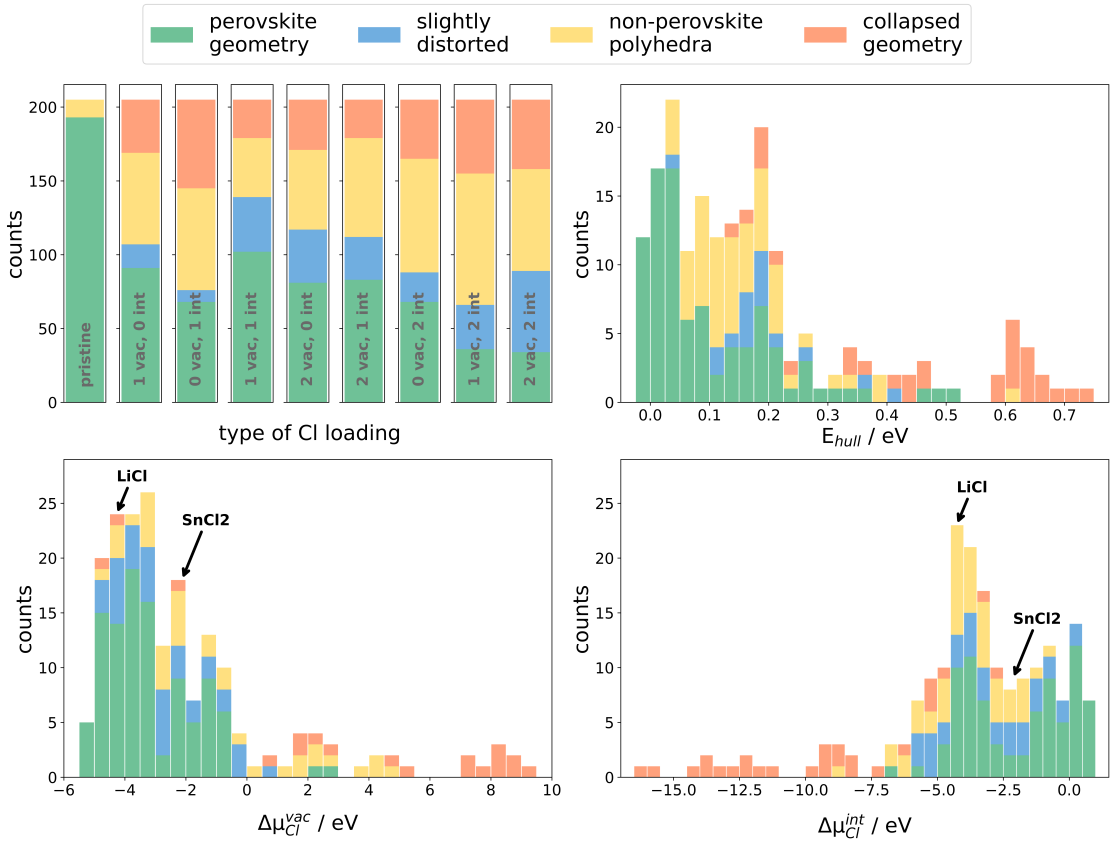

Fig. 5: a) Histogram displaying the classification of the analyzed configurations into perovskite geometry, slightly distorted perovskites, a different framework of polyhedra, or fully collapsed structures. b) Histogram of E_{hull} for all pristine geometries. The color coding refers to the configuration with one vacancy and one interstitial. c)/d) Histograms with respect to $\mu_{Cl}^{vac/int}$ associated with the introduction of one vacancy/interstitial. The color coding refers to the corresponding intercalation configurations.

every DFT optimized configuration visually and decided whether it exhibits (i) perovskite geometry according to the definition given here, (ii) only slight distortions to the perovskite geometry in the vicinity of the defects, (iii) a different network of connected cation polyhedra or (iv) a fully collapsed geometry, for instance a clustering of metals or a cleavage within the configuration. Admittedly, this approach entails some arbitrariness.

The results of this visual classification are depicted in Fig. 5 a). Out of the 205 investigated pristine compounds the vast majority of 193 geometries retained their perovskite geometry during the relaxation, the remainder was ascribed to the class of non-perovskite polyhedra. The picture changes significantly as soon as the other types of Cl loadings are

considered. The introduction of charge neutral defects, i.e. one (two) vacancy-interstitial pair(s), reduces the number of compounds with retained perovskite geometry or only slight distortions to 106 (76). Regarding charged defects, vacancies have lower destabilizing effect than interstitials as the introduction of one (two) vacancy(ies) leads to 139 (111) relaxed structures with perovskite geometry including slight distortions whereas the introduction of one (two) interstitial(s) results in only 117 (89). As discussed in the previous paragraph structural changes indicate instability. Hence, we do not consider the non-perovskite and the fully collapsed geometries as potentially stable perovskites entailing major consequences for any subsequent analysis. Furthermore, it is noteworthy that we observed the annihilation of vacancy-interstitial pairs during relaxation in many cases.

Fig. 5 b) depicts the distribution of the stability descriptor E_{hull} for the set of 193 pristine compounds with perovskite geometry. We would like to emphasize that a compelling prediction of a material's synthesizability is not possible due to the incompleteness of the underlying database, imperfections of DFT, the negligence of any kinetic effect, and unknown complications in the synthesis procedure.[58] Nevertheless, values of a few tens meV/atom indicate a high likelihood for synthesizability, whereas stable materials have also been found for up to roughly $E_{hull} \approx 200$ meV/atom,[84,85] as temperature, pressure or suitable dopants may provide stabilizing effects. In the present dataset 29 materials with $E_{hull} < 25$ meV/atom with a high chance of synthesizability could be identified, comprising 18 of the 24 compounds which were suggested by a previous screening study concentrating only on stoichiometric ABX_3 perovskites[81] - the remaining six lying slightly above the 25meV threshold in our investigation. Consequently, we propose 11 additional stable compounds with $NaAgCl_3$, $KSnCl_3$, $RbCuCl_3$, $CsCuCl_3$, and $InCaCl_3$ being particularly remarkable as they are predicted to lie on the convex hull of stability, i.e. $E_{hull} = 0$. We speculate that these compounds were not found in the earlier study[81] as octahedral tiltings and distortions were not considered as comprehensively as in our present work.

The color coding in Fig. 5 b) refers to the phase with one vacancy-interstitial pair. The graph shows a correlation between the value of E_{hull} of the pristine material and the tendency of the phase with the vacancy-interstitial pair to preserve perovskite geometry. In particular, none of the compounds with $E_{hull} > 500$ meV/atom remained in the perovskite structure when the vacancy-interstitial pair was introduced. Apparently, the defect leads to a symmetry breaking of the geometry enabling the optimization algorithm to find a ground state configuration which is lower in energy than the pristine perovskite indicating the instability of the latter.

Note that the importance of considering the stability as a function of $\mu_{Cl}^{vac/int}$ for potential battery materials has been highlighted above and its determination following equation 3 and as summarized in Fig. 5 c) and d) is considered one of the major purposes of this study. In these figures, again, the data are classified according to the relaxed geometry, in this case after introduction of one vacancy/interstitial. The figures show that the majority of defects lead to Cl chemical potentials of $-6.0 \leq \Delta\mu_{Cl}^{vac/int} \leq 1.0$ eV. In particular, the data outside this range almost exclusively corresponds to configurations that are either fully collapsed or arranged in some non-perovskite framework and not considered in the present study. Recalling equations 1 and 2, $\mu_{Cl}^{vac/int}$ can be used to decide whether the intercalation thermodynamics of a certain compound allow for potential usability as anode, solid electrolyte or cathode —keeping in mind that this is by far not the only requirement from a material's perspective. To facilitate the classification $\Delta\mu_{Cl}^{LiCl}$ and $\Delta\mu_{Cl}^{SnCl_2}$, i.e. the Cl chemical potential of the reference systems LiCl and $SnCl_2$, are marked in Fig. 5 c) and d).

Regarding only the configurations with retained perovskite geometry or minor distortions, the distribution of $\Delta\mu_{Cl}^{vac}$ is slightly shifted towards more negative values compared to $\Delta\mu_{Cl}^{int}$, giving rise to a vast amount of compounds with rather low values for $\Delta\mu_{Cl}^{vac}$. In these compounds, the energy necessary for vacancy creation is rather high, what is desirable in anode materials or solid electrolytes. The five compounds with $\Delta\mu_{Cl}^{vac} < -5$ eV are $CsCaCl_3$, $KCaCl_3$, $KSrCl_3$, $RbCaCl_3$, and $RbSrCl_3$. On the other hand, many compounds are found

with $\Delta\mu_{Cl}^{vac} > -2.5$ eV which is the range of suitable cathode materials manifesting $\phi_{OCV} >$ 2.0 V vs. Li/Li^+ but also a requirement for solid electrolytes. $CsNiCl_3$, $KGaCl_3$, $NaAgCl_3$, and $RbNiCl_3$ appear particularly interesting with values close to $\Delta\mu_{Cl}^{vac} = -0.5$ eV. The two outliers with $\Delta\mu_{Cl}^{vac} > 2.0$ eV are $BiLiCl_3$ and $GaEuCl_3$. The distribution of $\Delta\mu_{Cl}^{int}$ exhibits less values in the range of potential anodes but is somewhat stronger pronounced in the region $\Delta\mu_{Cl}^{int} > -2.5$ eV. $CsMgCl_3$, $KMgCl_3$, $NaMgCl_3$, $RbMgCl_3$, and $SrLiCl_3$, for instance, appear interesting as they are located around $\Delta\mu_{Cl}^{int} = 1.0$ eV.

Within our study over 200 chloride perovskites were analyzed concerning their stability and intercalation chemistry. Yet, a full thermodynamic picture for a potential future battery material can only be obtained by combining the requirements on both aspects, while reviewing and interpreting the relevant entities individually for each material can be a tedious and error-prone task. Furthermore, the stability information provided by the E_{hull} analysis is incomplete, as it is grounded on gas phase Cl_2 as reference system and does not allow non-stoichiometric decomposition. The electrochemical conditions within a battery setup may though differ significantly from standard conditions (i.e., $\Delta\mu_{Cl} = 0$) as Fig. 5 c) and d) demonstrate, and the Cl loading is obviously not necessarily fixed in a battery material. The analysis based on grand canonical diagrams provides remedy regarding these issues by capturing all relevant information within a single graph and, thus, enabling visual and intuitive access to the matter at one glance. $InCaCl_3$ is a good example of how misleading a naive approach not considering the whole picture can be as discussed further down (Fig. 6 f).

For further analysis we generated the grand canonical diagrams for all 205 investigated perovskites as described in the methodological section (equation 6) and of which a selection of eight diagrams is depicted in Fig. 6. These exemplary diagrams will be thoroughly discussed in the following paragraphs while it will be highlighted that the conclusions drawn here can be directly transferred to other materials with the corresponding diagrams in Fig. S1, S2, S3, and S4 in the SI. Additionally, the grand canonical diagrams on all 205 investigated

perovskites including the full list of decomposition products is attached to the corresponding DFT calculations which can be accessed through the NOMAD repository[86] as stated in the data availability statement. All diagrams follow the scheme depicted in Fig. 3. The green, blue, yellow, and orange curves correspond to the (chlorinated/dechlorinated) perovskites, where the color coding corresponds to the level of distortion of the relaxed geometry as in Fig. 5. Note that in the majority of cases differing start configurations of equal stiochiometry converged into the same ground state and can, thus, not be distinguished anymore in the diagrams. The red curves represent allotropes and decomposition products as labeled.

Fig. 6 a) presents the grand canonical diagram of the potential cathode material $CsAgCl_3$. Perovskite geometry was preserved for all intercalation configurations, only the introduction of two interstitials resulted in a slight deviation (blue curve). As discussed in the methodological section, the theoretical OCV, which is related to a certain transition, can be associated with the intersection of the corresponding curves. The OCV related to the transition from $CsAgCl_3$ to $CsAgCl_{2.75}$ is highlighted by the purple area in the graph and amounts to 3.22 V vs. Li/Li^+, while no transition to $CsAgCl_{2.875}$ occurs. Slightly below at 3.02 V occurs the transition from the dechlorinated perovskite $CsAgCl_{2.75}$ to $CsAgCl_2$ and subsequently to 0.5 Ag + 0.5 Cs_2AgCl_3 and Ag + CsCl. Such conversion reactions have been associated with irreversible and undesirable capacity fading.[47,87] Regarding increased potential, the analysis predicts a conversion reaction from $CsAgCl_3$ to 0.5 Ag_2Cl_{13} + $CsCl_5$ and 0.5 Ag_2Cl_{13} + $CsCl_8$ at 3.73 V and 3.88 V, preventing the stabilization of interstitials in $CsAgCl_3$. Eventually, the creation of vacancies within $CsAgCl_3$ is associated with a potential of 3.22 V. In addition, our investigations suggest that for reversible cycling the potential should not be lowered to less than 3.02 V and not be raised above 3.73 V in order to prevent decomposition of the material. This rather small range for potential cycling makes this compound not suitable as a possible cathode material.

The diagram of $RbCuCl_3$ in Fig. 6 b) can be analyzed quite similarly. Here, both the introduction of one and two interstitials result in slight distortion of the perovskite phase.

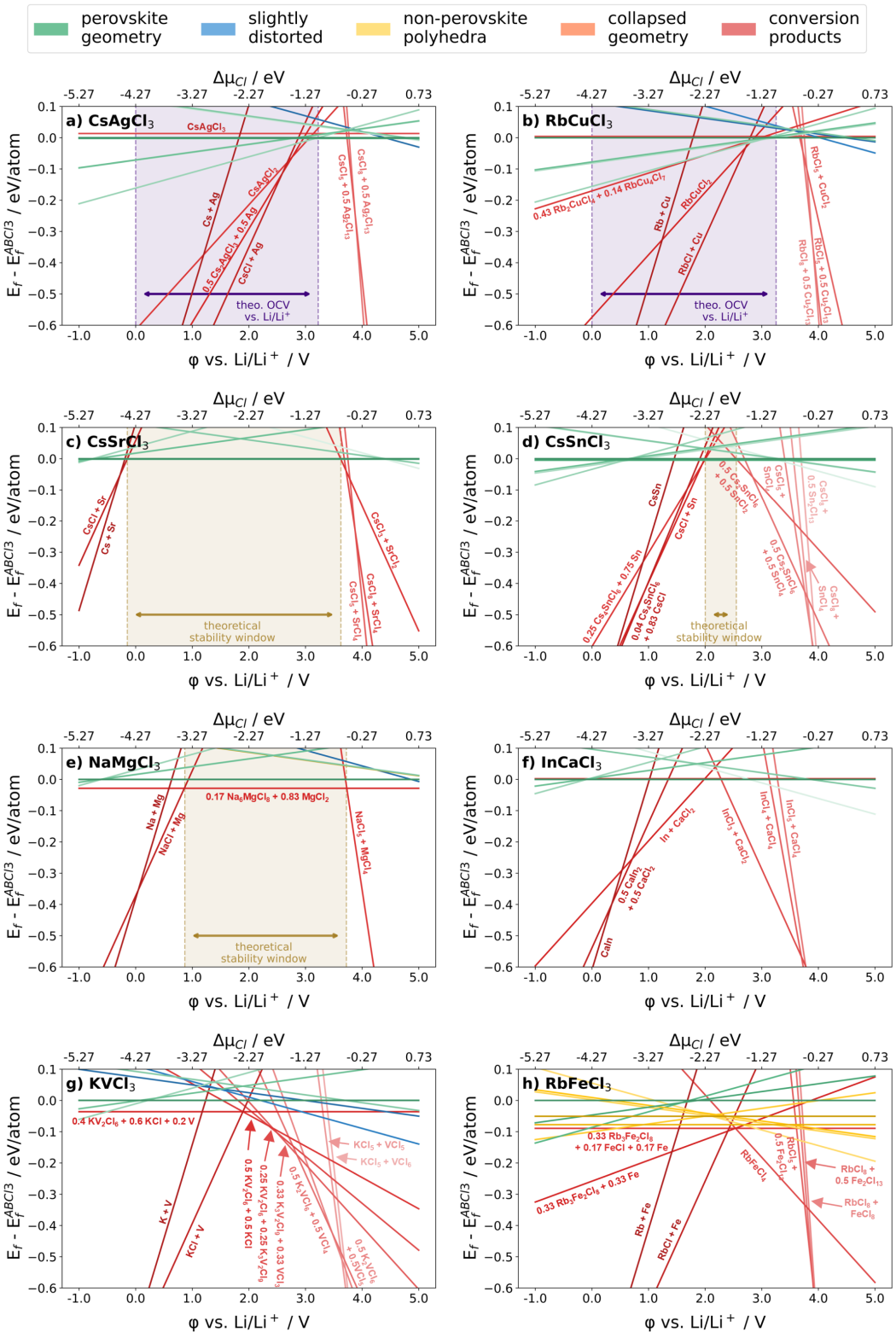

Fig. 6: Grand canocical diagrams for eight exemplary compounds. The theoretical open circuit voltage and the theoretical stability window are highlighted in the corresponding figures.

The transitions from $RbCuCl_3$ to $RbCuCl_{2.875}$ and then $RbCuCl_{2.75}$ occur at the theoretical OCVs of 3.25 V and 2.98 V before conversion reactions to RbCuCl2 and RbCl + Cu appear by further lowering the potenial to 2.79 V and 2.71 V. As in the case of $CsAgCl_3$, increasing the potential should not result in chlorination of $RbCuCl_3$ but rather in conversion reactions. Here, reversible deintercalation is thermodynamically possible within the range of 2.79 V and 3.22 V.

It is one declared aim of the present study to predict intercalation reactions within perovskite materials as presented in the paragraphs above for vacancy formation within $CsAgCl_3$ and $RbCuCl_3$. Such topotactic solid state reactions suggest reversible deintercalation of Cl and are a prerequisite for promising cathode materials. We found that $CsCuCl_3$, $RbAgCl_3$, $KAgCl_3$, and $KCuCl_3$ (Fig. S1) exhibit similar behavior as their counterparts $CsAgCl_3$ and $RbCuCl_3$, although in the cases of $KAgCl_3$ and $KCuCl_3$ the stabilization of vacancies is not directly predicted, as the corresponding structures are energetically unfavorable by a few meV/atom compared to a conversion reaction. Nevertheless, this magnitude is not significant given the applied level of theory and the dechlorinated configurations could still turn out to be stabilized.

The diagram in Fig. 6 c) presents a fundamentally different picture. The pristine compound is stabilized over a wide potential range from -0.15 V to 3.62 V. This theoretical stability window is constrained by conversion reactions into CsCl + Sr at the lower and $CsCl_3$ + $SrCl_2$ at the upper end. Topotactic reactions of the pristine material into chlorinated/dechlorinated perovskites are energetically unfavorable throughout. This diagram reveals almost ideal thermodynamics for a solid electrolyte material which should neither decompose by topotactic nor conversion reactions. Fig. 6 d) shows the grand canonical diagram of the recently discussed solid electrolyte $CsSnCl_3$.[88–91] The stability window is far narrower only ranging from 2.0 V to 2.55 V decomposing to 0.25 Cs_4ScCl_6 + 0.75 Sn and CsCl + Sn at lower and to 0.5 Cs_2SnCl_6 + 0.5 $SnCl_2$ at higher potentials. Interestingly, this is in strong contrast to the experiments by Xia et al. who reported a stable range of

6.1 V.[88] A similar mismatch of the theoretical and experimental stability windows has also been found for popular Li ion conductors, where it was explained with stabilizing conversion products at the interfaces between solid electrolyte and electrodes.[44,46] In conclusion, we also consider materials with stability windows down to 0.5 V as potential solid electrolytes. Eventually, we suggest $CsCaCl_3$, $KCaCl_3$, $KSnCl_3$, $NaCaCl_3$, $NaSnCl_3$, $RbCaCl_3$, $RbSnCl_3$, and $RbSrCl_3$ as promising candidate materials (Fig. S2) in addition to $CsSnCl_3$ and $CsSrCl_3$ as presented here.

Fig. 6 e) belongs to $NaMgCl_3$, a material which is in principle predicted unstable as the decomposition into 0.17 Na_6MgCl_8 + 0.83 $MgCl_2$ is energetically favourable by E_{hull} = 29 meV/atom. Still, as discussed at different points of this essay, this magnitude is clearly within the range of likely stability. Therefore, $NaMgCl_3$ is reported here as potential solid electrolyte material due to its wide stability window ranging from 0.87 V to 3.72 V outside of which it converts into NaCl+Mg and $NaCl_5$ + $MgCl_4$. The materials $BaLiCl_3$, $CsBaCl_3$, $KBaCl_3$, $KMgCl_3$, $KMnCl_3$, $LiSnCl_3$, $NaCuCl_3$, $NaMnCl_3$, $RbBaCl_3$, $RbMgCl_3$, $RbMnCl_3$, and $SrLiCl_3$ exhibit similar thermodynamic features (Fig. S3 and S4).

$InCaCl_3$, which is analysed in Fig. 6 f), is likely to be stable, yet in electrochemical conditions as within a battery it decomposes to a variety of binaries throughout almost the entire potential range. Please note that this material exhibits $E_{hull} = 0$ and $\mu_{Cl}^{vac} = -4.40$ eV/ $mu_{Cl}^{int} = -0.41$ eV. Hence, without the comprehensive picture revealed by the grand canonical analysis, such a material could have been falsely suggested as solid electrolyte material. The diagram of $KVCl_3$ as in Fig. 6 g) exhibits similar features, only that the decomposition into 0.4 KV_2Cl_6 + 0.6 KCl + 0.2 V imposes a non-zero value of E_{hull} = 36 meV/atom. This value is not too high to exclude synthesizability. Yet, the grand canonical diagram reveals how unlikely the stabilization of any chlorinated or dechlorinated perovskite geometry is and that the decomposition into a variety of products at all relevant potentials is to be expected. Finally, regarding $RbFeCl_3$ presented in Fig. 6 h), most of the intercalation geometries became highly distorted (yellow and orange curves) and energetically favourable

decompositions are found throughout the diagram. Both aspects indicate very low chance of synthesizability. All compounds which have not been discussed above as potential cathodes or solid electrolytes fall into these last three categories and are unlikely to be of any use for CIBs.

Some final remarks on the results shall be given: The stabilization of Cl vacancies or Cl interstitials in chloride perovskites of the kind $ABCl_3$ seems to be a very rare feature. The only stable vacancies in the entire dataset were exhibited by the compounds discussed (and eventually rejected) as cathode materials above. No potential anode materials could be proposed within the investigated compounds as for any compound with low μ_{Cl}^{vac} like in $InCaCl_3$, some conversion reaction is energetically more favourable rendering the material unsuitable as anode. Furthermore, we did not find any stabilized interstitial across the whole dataset rendering the existence of such species very unlikely.

Conclusion

In order to accelerate the advancement of CIBs, in the present study we investigated the entire class of ternary chloride perovskites with stoichiometry $ABCl_3$ to discover potential electrode and solid electrolyte materials. To this end, we focused on the intercalation thermodynamics, which reveal particularly important properties for the determination of promising materials as comprehensively discussed. After having filtered the potentially stable 205 compounds from databases and descriptors, a state-of-the-art MLIP was used to screen 18782 potential intercalation configurations $ABCl_{3\pm x}$ with $x \in \left\{0, \frac{1}{24}, \frac{1}{12}\right\}$ for each compound, out of which the ones lowest in energy were used for further DFT investigations. A small benchmark of the MLIP was conducted, which revealed that, although the absolute energies of the considered configurations differed by up to 50 meV/atom (sometimes even higher), the energetic order of the configurations prevailed in the majority of cases when moving from MLIP to DFT evaluation.

The DFT energies were used to evaluate the stability descriptor E_{hull} as well as the Cl chemical potential associated with Cl vacancies or Cl interstitials $\mu_{Cl}^{vac/int}$. Many compounds lying on the convex hull or only slightly above could be identified, while the chemical potential for chlorination/dechlorination was distributed between approximately 0 to -6 eV, which is also the relevant range for battery materials. A deep understanding of the thermodynamics of each compound could be gained through the generation of grand canonical diagrams. We found that hardly any Cl vacancies and no Cl interstitials were stabilized in the perovskite structure, the conversion into other compounds being energetically favorable in the absolute majority of cases. This also means that reversible intercalation/deintercalation is unlikely in most compounds. The few exceptions with stabilized vacancies, namely $CsAgCl_3$, $CsCuCl_3$, $KAgCl_3$, $KCuCl_3$, $RbAgCl_3$, and $RbCuCl_3$ are in principle potential candidates for cathode materials, although reversible cycling should be possible only in rather narrow potential ranges which reneders them eventually unsuitable. For solid electrolyte materials on the other hand, we could identify 23 candidates exhibiting promising thermodynamics, as for instance $CsSrCl_3$, $CsSnCl_3$, $KCaCl_3$, $NaMgCl_3$, and $SrLiCl_3$, to name only a few. None of the 205 compounds suffices the thermodynamic requirements of CIB anode materials.

The conducted investigation not only identifies a number of potential materials but also presents a screening approach which, we believe, illuminates the thermodynamics in a particularly comprehensive fashion in two ways: (i) Unlike strategies that probe only a limited amount of configurations, which are typically created by intuition, in this study we comprehensively sampled the configurational space of the intercalation compounds. The evaluation with the aid of the MLIP renders it rather unlikely that an important configuration is missed out. (ii) The inclusive investigation of all relevant thermodynamic properties in the grand canonical analysis enables intuitive access to the matter which can hardly be gained otherwise. In only one figure grand canonical diagrams contain information on the relative stability of the pristine and chlorinated/dechlorinated perovskites as well as potential decomposition products at varying potentials and Cl loadings. This is remarkable as a quick

glimpse at the diagram shows at which potential chlorination/dechlorination takes place and whether topotactic or conversion reactions are to be expected, immediately revealing the thermodynamic suitability of a material as a anode, cathode, or solid electrolyte material. Furthermore, the relevant thermodynamic properties as the OCV or the electrochemical stability window can be read off directly from the diagrams. We would like to emphasize that the entire strategy can be transferred to any other class of materials and any other shuttle ion e.g. Li^+ or Na^+.

Nonetheless, one drawback in the presented approach was that many perovskite geometries collapsed during relaxation, particularly after the introduction of vacancies or interstitials. We interpret this as indication for instability. Still, information on the degree of instability of the chlorinated/dechlorinated perovskite, i.e. the defect formation energy, would allow an estimation on the likelihood of the occurrence of such potentially metastable species, for instance through thermal excitation. This could be achieved through suitable constraints for geometry optimization which would prevent structural collapse, although defining these will be a rather complicated task, given the vast amount of differing distortions and types of Cl loading that have to be considered. Similarly, the formation energy for self-interstitials would be insightful, for instance to estimate the amount of mobile species in a solid electrolyte material, but the lowest energy configuration of the MLIP screening that we analyzed with DFT typically relaxed to the pristine ground state for all relevant materials. So the formation energy for a self-interstitial could be gained by DFT evaluation of configurations which had turned out to be energetically elevated in the MLIP run. Please note also that on the microscopic scale defects can be locally positively or negatively charged with the compensating charge located somewhere else within the necessarily overall charge neutral unit cell, which, however, has not been analyzed in further detail here.

Eventually, we would like to emphasize that the intercalation thermodynamics investigated in the present study are only one necessary requirement for the purpose of a battery material. For a serious theoretical proposal of a material other properties have to be eval-

uated as well. First and foremost, high ionic conductivity is a prerequisite for electrodes as well as solid electrolytes which can typically be indicated by low diffusion barriers as obtained in nudged elastic band calculations or by ab-initio molecular dynamics simulations. Furthermore, electrodes should conduct electronic currents while solid electrolytes must not. Indications can be found through the evaluation of the band gap of the material obtained in density of states calculations. Mechanical stress and strain is frequently blamed for the evolution of cracks and eventual pulverization of the material. Corresponding mechanical properties may thus be of great relevance, too.

In the end, we have demonstrated that the grand canonical approach for the analysis of battery materials is particularly advantageous with respect to the question whether intercalation/deintercalation processes or conversion reactions can occur in battery materials under operating conditions. The application of this approach to the class of chloride perovskites revealed a number of thermodynamically promising candidate materials. Yet, we emphasize that further investigations are required for the ultimate proposal of new materials, which we suggest for future studies.

Supporting Information

Supporting Information is available online or from the authors.

Acknowledgements

This work contributes to the research performed at the Center for Electrochemical Energy Storage Ulm-Karlsruhe (CELEST) and was supported by the German Research Foundation (DFG) under project ID 390874152 (POLiS Cluster of Excellence) and the Dr. Barbara Mez-Starck Foundation. The authors acknowledge computer time provided by the state of Baden-Württemberg through bwHPC and the German Research Foundation (DFG) through grant no INST 40/575-1 FUGG (JUSTUS 2 cluster).

Last but not least, we sincerely thank Jonathan Schmidt for the screening of the Alexandria database for perovskite-like compounds which we used as input for the present study.[77,78,80]

Conflict of Interest

The authors declare no conflict of interest

Data Availability Statement

All electronic structure calculations used in this work are made available under the Creative Commons Attribution license (CC BY 4.0) on the NOMAD repository (https://nomad-lab.eu) within the dataset "Chloride_Perovskites_GranCan": https://doi.org/10.17172/nomad.hsf1-hngb.

References

(1) Goodenough, J. B.; Park, K. The Li-Ion Rechargeable Battery: A Perspective. *Journal of the American Chemical Society* **2013**, *135*, 1167–1176.

(2) Tarascon, J. The Li-Ion Battery: 25 Years of Exciting and Enriching Experiences. *ECS Interface* **2016**, *25*, 79–83.

(3) Li, M.; Lu, J.; Chen, Z.; Amine, K. 30 Years of Lithium-Ion Batteries. *Advanced Materials* **2018**, *30*, 1800561.

(4) Whittingham, M. S.; Xiao, J. Fifty Years of Lithium-ion Batteries and What is Next? *MRS Bulletin* **2023**, *48*, 1118–1124.

(5) Whittingham, M. S. Electrical energy storage and intercalation chemistry. *Science* **1976**, *192*, 1126–1127.

(6) Mizushima, K.; Jones, P. C.; Wiseman, P. J.; Goodenough, J. B. LixCoO2 - A new cathode material for batteries of high energy density. *Materials Research Bulletin* **1980**, *15*, 783–789.

(7) Tarascon, J.-M.; Armand, M. Issues and challenges facing rechargeable lithium batteries. *Nature* **2001**, *414*, 359–367.

(8) Yoshino, A. The Birth of the Lithium-Ion Battery. *Angewandte Chemie International Edition* **2012**, *51*, 5798–5800.

(9) Liu, Z.; Yu, A.; Lee, J. Synthesis and characterization of $LiNi_{1-x-y}Co_xMn_yO_2$ as the cathode materials of secondary lithium batteries. *Journal of Power Sources* **1999**, *81*, 416–419.

(10) Ohzuku, T.; Makimura, Y. Layered Lithium Insertion Material of $LiCo_{1/3}Ni_{1/3}Mn_{1/3}O_2$ for Lithium-Ion Batteries. *Chemistry Letters* **2001**, *30*, 642–643.

(11) Whittingham, M. S. Lithium Batteries and Cathode Materials. *Chemical Reviews* **2004**, *104*, 4271–4301.

(12) Blomgren, G. E. The Development and Future of Lithium Ion Batteries. *Journal of The Electrochemical Society* **2016**, *164*, A5019.

(13) Koech, A. K.; Mwandila, G.; Mulolani, F. A review of improvements on electric vehicle battery. *Heliyon* **2024**, *10*, e34806.

(14) Padhi, A.; Nanjundaswamy, K.; Masquelier, C.; Okada, S.; Goodenough, J. Effect of Structure on the Fe^{3+}/Fe^{2+} Redox Couple in Iron Phosphates. *Journal of The Electrochemical Society* **1997**, *144*, 1609–1613.

(15) Whittingham, M. S. Ultimate Limits to Intercalation Reactions for Lithium Batteries. *Chemical Reviews* **2014**, *114*, 11414–11443.

(16) Fichtner, M. Recent Research and Progress in Batteries for Electric Vehicles. *Batteries & Supercaps* **2021**, *5*, e202100224.

(17) Moskowitz, S. L. *The Advanced Materials Revolution: Technology and Economic Growth in the Age of Globalization*; John Wiley & Sons, 2009.

(18) Ortner, H. M.; Ettmayer, P.; Kolaska, H. The history of the technological progress of hardmetals. *International Journal of Refractory Metals and Hard Materials* **2014**, *44*, 148–159.

(19) Cho, J.; Park, J. H.; Kim, J. K.; Schubert, E. F. White light-emitting diodes: history, progress, and future. *Laser & photonics reviews* **2017**, *11*, 1600147.

(20) Beretta, D. et al. Thermoelectrics: From history, a window to the future. *Materials Science and Engineering: R: Reports* **2019**, *138*, 100501.

(21) Kim, J.; Campbell, A. S.; de Ávila, B. E.-F.; Wang, J. Wearable biosensors for healthcare monitoring. *Nature Biotechnology* **2019**, *37*, 389–406.

(22) Rothemund, P.; Kim, Y.; Heisser, R. H.; Zhao, X.; Shepherd, R. F.; Keplinger, C. Shaping the future of robotics through materials innovation. *Nature Materials* **2021**, *20*, 1582–1587.

(23) Post Lithium Storage (POLIS) - Cluster of Excellence. 2017; https://www.postlithiumstorage.org.

(24) Esser, B.; Ehrenberg, H.; Fichtner, M.; Groß, A.; Janek, J. Post-Lithium Storage—Shaping the Future. *Advanced Energy Materials* **2025**, *15*, 2402824.

(25) Gschwind, F.; Euchner, H.; Rodriguez-Garcia, G. Chloride Ion Battery Review: Theoretical Calculations, State of the Art, Safety, Toxicity, and an Outlook towards Future Developments. *European Journal of Inorganic Chemistry* **2017**, *2017*, 2784–2799.

(26) Karkera, G.; Reddy, M. A.; Fichtner, M. Recent developments and future perspectives of anionic batteries. *Journal of Power Sources* **2021**, *481*, 228877.

(27) Zhao, X.; Ren, S.; Bruns, M.; Fichtner, M. Chloride ion battery: A new member in the rechargeable battery family. *Journal of Power Sources* **2014**, *245*, 706–711.

(28) Jain, A.; Ong, S. P.; Hautier, G.; Chen, W.; Richards, W. D.; Dacek, S.; Cholia, S.; Gunter, D.; Skinner, D.; Ceder, G.; Persson, K. A. The Materials Project: A materials genome approach to accelerating materials innovation. *APL Materials* **2013**, *1*, 011002.

(29) Hautier, G. Finding the needle in the haystack: Materials discovery and design through computational ab initio high-throughput screening. *Computational Materials Science* **2019**, *163*, 108–116.

(30) Deringer, V. L.; Caro, M. A.; Csányi, G. Machine Learning Interatomic Potentials as Emerging Tools for Materials Science. *Advanced Materials* **2019**, *31*, e1902765.

(31) Reuter, K.; Scheffler, M. Composition, structure, and stability of $RuO_2(110)$ as a function of oxygen pressure. *Phys. Rev. B* **2001**, *65*, 035406.

(32) Nørskov, J. K.; Rossmeisl, J.; Logadottir, A.; Lindqvist, L.; Kitchin, J. R.; Bligaard, T.; Jónsson, H. Origin of the Overpotential for Oxygen Reduction at a Fuel-Cell Cathode. *J. Phys. Chem. B* **2004**, *108*, 17886–17892.

(33) Gossenberger, F.; Juarez, F.; Groß, A. Sulfate, Bisulfate, and Hydrogen Co-adsorption on Pt(111) and Au(111) in an Electrochemical Environment. *Front. Chem.* **2020**, *8*, 634.

(34) Groß, A. Grand-canonical approaches to understand structures and processes at electrochemical interfaces from an atomistic perspective. *Current Opinion in Electrochemistry* **2021**, *27*, 100684.

(35) Green, M. A.; Ho-Baillie, A.; Snaith, H. J. The emergence of perovskite solar cells. *Nature Photonics* **2014**, *8*, 506–514.

(36) Jena, A.; Kulkarni, A.; Miyasaka, T. Halide Perovskite Photovoltaics: Background, Status, and Future Prospects. *Chemical Reviews* **2019**, *119*, 3036–3103.

(37) Moia, D.; Maier, J. Ion Transport, Defect Chemistry, and the Device Physics of Hybrid Perovskite Solar Cells. *ACS Energy Letters* **2021**, *6*, 1566–1576.

(38) Euchner, H.; Groß, A. Atomistic modeling of Li- and post-Li-ion batteries. *Physical Review Materials* **2022**, *6*, 040302.

(39) Groß, A.; Sakong, S. Modelling the electric double layer at electrode-electrolyte interfaces. *Current Opinion in Electrochemistry* **2019**, *14*, 1–6.

(40) Gossenberger, F.; Roman, T.; Groß, A. Hydrogen and halide co-adsorption on Pt(111) in an electrochemical environment: a computational perspective. *Electrochimica Acta* **2016**, *216*, 152–159.

(41) Rahmani Didar, B.; Yashina, L.; Groß, A. First-Principles Study of the Surfaces and Equilibrium Shape of Discharge Products in Li–Air Batteries. *ACS Applied Materials & Interfaces* **2021**, *13*, 24984–24994.

(42) Huang, J.; Li, M.; Eslamibidgoli, M. J.; Eikerling, M.; Groß, A. Cation Overcrowding Effect on the Oxygen Evolution Reaction. *JACS Au* **2021**, *1*, 1752–1765.

(43) Sarkar, K.; Hübner, D.; Stottmeister, D.; Groß, A. Unraveling the intricacies of surface salt formation on Mg(0001): Implications for chloride-ion batteries. *Physical Review Materials* **2024**, *8*, 015401.

(44) Zhu, Y.; He, X.; Mo, Y. Origin of Outstanding Stability in the Lithium Solid Electrolyte Materials: Insights from Thermodynamic Analyses Based on First-Principles Calculations. *ACS Applied Materials & Interfaces* **2015**, *7*, 23685–23693.

(45) Zhu, Y.; He, X.; Mo, Y. First principles study on electrochemical and chemical stability of solid electrolyte–electrode interfaces in all-solid-state Li-ion batteries. *Journal of Materials Chemistry A* **2016**, *4*, 3253–3266.

(46) Richards, W. D.; Miara, L. J.; Wang, Y.; Kim, J. C.; Ceder, G. Interface Stability in Solid-State Batteries. *Chemistry of Materials* **2016**, *28*, 266–273.

(47) Panja, S.; Miao, Y.; Döhn, J.; Choi, J.; Fleischmann, S.; Chandrappa, S. G.; Diemant, T.; Groß, A.; Karkera, G.; Fichtner, M. Synthesis, Structural Analysis, and Degradation Behavior of Potassium Tin Chloride as Chloride-Ion Batteries Conversion Electrode Material. *Advanced Functional Materials* **2024**, *35*, 2413489.

(48) Schmickler, W.; Santos, E. *Interfacial Electrochemistry*, 2nd ed.; Springer, 2010.

(49) Binninger, T.; Marcolongo, A.; Mottet, M.; Weber, V.; Laino, T. Comparison of computational methods for the electrochemical stability window of solid-state electrolyte materials. *J. Mater. Chem. A* **2020**, *8*, 1347–1359.

(50) Sotoudeh, M.; Baumgart, S.; Dillenz, M.; Döhn, J.; Forster-Tonigold, K.; Helmbrecht, K.; Stottmeister, D.; Groß, A. Ion Mobility in Crystalline Battery Materials. *Advanced Energy Materials* **2024**, *14*, 2302550.

(51) Bölle, F. T.; Mathiesen, N. R.; Nielsen, A. J.; Vegge, T.; García Lastra, J. M.; Castelli, I. E. Autonomous Discovery of Materials for Intercalation Electrodes. *Batteries & Supercaps* **2020**, *3*, 488–498.

(52) Helmbrecht, K.; Euchner, H.; Groß, A. Revisiting the Chevrel Phase: Impact of Dispersion Corrections on the Properties of Mo6S8 for Cathode Applications. *Batteries & Supercaps* **2022**, *5*, e202200002.

(53) Baumgart, S.; Groß, A.; Sotoudeh, M. Data-Driven Site Occupancy Statistics in Cubic Prussian Blue. *ACS Physical Chemistry Au* **2025**, *5*, 346–355.

(54) Glazer, A. M. A brief history of tilts. *Phase Transitions* **2011**, *84*, 405–420.

(55) Howard, C. J.; Stokes, H. T. Group-Theoretical Analysis of Octahedral Tilting in Perovskites. *Acta Crystallographica Section B Structural Science* **1998**, *54*, 782–789.

(56) Stokes, H. T.; Kisi, E. H.; Hatch, D. M.; Howard, C. J. Group-theoretical analysis of octahedral tilting in ferroelectric perovskites. *Acta Crystallographica Section B* **2002**, *58*, 934–938.

(57) Xie, N.; Zhang, J.; Raza, S.; Zhang, N.; Chen, X.; Wang, D. Generation of low-symmetry perovskite structures for ab initio computation. *Journal of Physics: Condensed Matter* **2020**, *32*, 315901.

(58) Döhn, J.; Groß, A. Computational Screening of Oxide Perovskites as Insertion-Type Cathode Material. *Advanced Energy and Sustainability Research* **2023**, *5*, 2300204.

(59) De Souza, R. A.; Kemp, D.; Wolf, M. J.; Ramadan, A. H. H. Caution! Static Supercell Calculations of Defect Migration in Higher Symmetry ABX_3 Perovskite Halides May Be Unreliable: A Case Study of Methylammonium Lead Iodide. *The Journal of Physical Chemistry Letters* **2022**, *13*, 11363–11368.

(60) Lufaso, M. W.; Woodward, P. M. Prediction of the crystal structures of perovskites using the software program SPuDS. *Acta Crystallographica Section B: Structural Science* **2001**, *57*, 725–738.

(61) Laakso, J.; Todorović, M.; Li, J.; Zhang, G.; Rinke, P. Compositional engineering of perovskites with machine learning. *Physical Review Materials* **2022**, *6*, 113801.

(62) Mannodi-Kanakkithodi, A.; Park, J.-S.; Martinson, A. B. F.; Chan, M. K. Y. Defect Energetics in Pseudo-Cubic Mixed Halide Lead Perovskites from First-Principles. *The Journal of Physical Chemistry C* **2020**, *124*, 16729–16738.

(63) Larsen, A. et al. The atomic simulation environment — a Python library for working with atoms. *Journal of Physics: Condensed Matter* **2017**, *29*, 273002.

(64) Behler, J.; Parrinello, M. Generalized Neural-Network Representation of High-Dimensional Potential-Energy surfaces. *Phys. Rev. Lett.* **2007**, *98*, 146401.

(65) Loew, A.; Sun, D.; Wang, H.; Botti, S.; Marques, M. A. L. Universal machine learning interatomic potentials are ready for phonons. *npj Computational Materials* **2025**, *11*, 178.

(66) Berger, E.; Bagheri, M.; Komsa, H.-P. Screening of Material Defects using Universal Machine-Learning Interatomic Potentials. *Small* **2025**, *21*, e03956.

(67) Batatia, I. et al. A foundation model for atomistic materials chemistry. *The Journal of Chemical Physics* **2025**, *163*, 184110.

(68) Schmidt, J.; Cerqueira, T.; Romero, A.; Loew, A.; Jäger, F.; Wang, H.; Botti, S.; Marques, M. Improving machine-learning models in materials science through large datasets. *Materials Today Physics* **2024**, *48*, 101560.

(69) Riebesell, J.; Goodall, R. E. A.; Benner, P.; Chiang, Y.; Deng, B.; Ceder, G.; Asta, M.; Lee, A. A.; Jain, A.; Persson, K. A. A framework to evaluate machine learning crystal stability predictions. *Nature Machine Intelligence* **2025**, *7*, 836–847.

(70) Perdew, J. P.; Burke, K.; Ernzerhof, M. Generalized Gradient Approximation Made Simple. *Phys. Rev. Lett.* **1996**, *77*, 3865–3868.

(71) Kresse, G.; Hafner, J. Ab initio molecular dynamics for liquid metals. *Physical Review B* **1993**, *47*, 558–561.

(72) Kresse, G.; Furthmüller, J. Efficiency of ab-initio total energy calculations for metals and semiconductors using a plane-wave basis set. *Computational Materials Science* **1996**, *6*, 15–50.

(73) Kresse, G.; Joubert, D. From ultrasoft pseudopotentials to the projector augmented-wave method. *Physical Review B* **1999**, *59*, 1758–1775.

(74) Blöchl, P. E. Projector augmented-wave method. *Phys. Rev. B* **1994**, *50*, 17953–17979.

(75) Bartel, C. J. Review of computational approaches to predict the thermodynamic stability of inorganic solids. *Journal of Materials Science* **2022**, *57*, 10475–10498.

(76) Wang, A.; Kingsbury, R.; McDermott, M.; Horton, M.; Jain, A.; Ong, S.; Dwaraknath, S.; Persson, K. A. A framework for quantifying uncertainty in DFT energy corrections. *Scientific Reports* **2021**, *11*, 15496.

(77) Schmidt, J.; Pettersson, L.; Verdozzi, C.; Botti, S.; Marques, M. A. L. Crystal graph attention networks for the prediction of stable materials. *Science Advances* **2021**, *7*, eabi7948.

(78) Schmidt, J.; Hoffmann, N.; Wang, H.; Borlido, P.; Carriço, P. J. M. A.; Cerqueira, T. F. T.; Botti, S.; Marques, M. A. L. Machine-Learning-Assisted Determination of the Global Zero-Temperature Phase Diagram of Materials. *Advanced Materials* **2023**, *35*, 2210788.

(79) Wu, M.; Lv, X.; Wang, J.; Wang, R.; Shi, X.; Zhang, H.; Jin, C.; Wei, Y.; Lian, R. High-throughput screening of TMOCl cathode materials based on the full-cell system for chloride-ion batteries. *Journal of Materials Chemistry A* **2021**, *9*, 23169–23177.

(80) Schmidt, J.; Shi, J.; Borlido, P.; Chen, L.; Botti, S.; Marques, M. A. L. Predicting the Thermodynamic Stability of Solids Combining Density Functional Theory and Machine Learning. *Chemistry of Materials* **2017**, *29*, 5090–5103.

(81) Körbel, S.; Marques, M. A. L.; Botti, S. Stability and electronic properties of new inorganic perovskites from high-throughput ab initio calculations. *Journal of Materials Chemistry C* **2016**, *4*, 3157–3167.

(82) Bartel, C. J.; Sutton, C.; Goldsmith, B. R.; Ouyang, R.; Musgrave, C. B.; Ghiringhelli, L. M.; Scheffler, M. New tolerance factor to predict the stability of perovskite oxides and halides. *Science Advances* **2019**, *5*, eaav0693.

(83) Ouyang, R. Exploiting Ionic Radii for Rational Design of Halide Perovskites. *Chemistry of Materials* **2019**, *32*, 595–604.

(84) Sun, W.; Dacek, S. T.; Ong, S.; Hautier, G.; Jain, A.; Richards, W. D.; Gamst, A. C.; Persson, K. A.; Ceder, G. The thermodynamic scale of inorganic crystalline metastability. *Science Advances* **2016**, *2*, e1600225.

(85) Chung, V.; Walsh, A.; Payne, D. J. Solid-state synthesizability predictions using positive-unlabeled learning from human-curated literature data. *Digital Discovery* **2025**, *4*, 2439–2453.

(86) Scheidgen, M. et al. NOMAD: A distributed web-based platform for managing materials science research data. *Journal of Open Source Software* **2023**, *8*, 5388.

(87) Karkera, G.; Soans, M.; Dasari, B.; Ediga, U.; Cambaz, M.; Meng, Z.; Diemant, T.; Fichtner, M. Tungsten Oxytetrachloride as a Positive Electrode for Chloride-Ion Batteries. *Energy Technology* **2022**, *10*, 2200193.

(88) Xia, T.; Li, Y.; Huang, L.; Ji, W.; Yang, M.; Zhao, X. Room-Temperature Stable Inorganic Halide Perovskite as Potential Solid Electrolyte for Chloride Ion Batteries. *ACS Applied Materials and Interfaces* **2020**, *12*, 18634–18641.

(89) Karkera, G.; Soans, M.; Akbaş, A.; Witter, R.; Euchner, H.; Diemant, T.; Cambaz, M. A.; Meng, Z.; Dasari, B.; Chandrappa, S. G.; Menezes, P. W.; Fichtner, M. A Structurally Flexible Halide Solid Electrolyte with High Ionic Conductivity and Air Processability. *Advanced Energy Materials* **2023**, *13*, 2300982.

(90) Xia, T.; Li, Q.; Zhao, X.; Shen, X. Bismuth and Chlorine Dual-Doped Perovskite Chloride as a Phase-Structure-Stable and Moisture-Resistant Solid Electrolyte for Chloride Ion Batteries. *Advanced Materials* **2024**, *36*, e2310565.

(91) Zhao, L.; Inoishi, A.; Miki, H.; Motoyama, M.; Okada, S.; Asano, T.; Sakuda, A.; Hayashi, A.; Sakaebe, H. Super Chloride Ionic Conductivity in $CsSnCl_3$-Based Perovskite Compound and Its Application for Solid-State Chloride Batteries. *Advanced Energy and Sustainability Research* **2024**, *5*, 2400198.